Nonlinear membrane-spring model for carbon nanotubes

M. Wang, X. Zhang,* and M. W. Lu
School of Aerospace, Tsinghua University, Beijing 100084, China
(Received 7 June 2005; revised manuscript received 29 August 2005; published 2 November 2005)

A nonlinear membrane-spring model, consisting of membranes connected by rotational springs, is proposed based on the physical structure of carbon nanotubes for simulating their mechanical response. In this model, the in-plane behavior of the graphite sheet is modeled by the membranes while its bending behavior is simulated by the rotational springs. Compared with the traditional shell model, it is more efficient and is easier to be coupled with the molecular dynamics method to develop a multiscale method. The mechanical behavior of carbon nanotubes is investigated by the incremental nonlinear static and dynamic analysis, and the numerical results agree well with those given by the molecular mechanics and other methods.

DOI: 10.1103/PhysRevB.72.205403 PACS number(s): 62.25.+g, 81.07.De

I. INTRODUCTION

Carbon nanotubes (CNTs) possess several predominant properties and their potential applications have attracted many researchers' attention. Generally speaking, experiments are the most straightforward means to explore the properties of materials. However, the small dimensions of CNTs pose challenges for the experimental determination of their mechanical behavior and properties, and most of these measurements[1–5] are made indirectly. As a result, computer simulation becomes more important than before. First-principle method and molecular dynamics (MD) have been widely used to predict the fundamental mechanical and electrical properties. For instance, the elastic and plastic properties of multiwalled nanotubes (MWNTs) under axial tension[6] were simulated by the MD method. Recently, Liew *et al.*[7] investigated the thermal stability of CNTs and found that the single-walled nanotubes (SWNTs) were thermally more stable than MWNTs. However, due to the limitation of computer capacities, these atomic methods are restricted to simulating CNTs with on the order of 10^6-10^8 atoms for a few nanoseconds, which greatly limits the size of CNTs' studying. Because of the prohibitive number of degrees of freedom in atomic scale simulation, the method based on the finite element implementation is an efficient method in some ways, especially for simulation of the large systems' mechanical response. The interesting phenomena, the rippling mode on the inner arc of the bent MWNTs observed in experiments,[2,3] were recurred in computational simulations based on the continuum theory.[8,9]

A SWNT can be thought of as one graphite sheet with hexagonal lattices that has been wrapped up into a seamless cylinder. CNTs, having a hollow structure, manifest themselves in dynamic properties of molecules, just like the macroscopic objects as shells. To employ the continuum shell theory in the analysis of the mechanical response of CNTs, the equivalent wall thickness and Young's module have to be determined. Fitting the energy of nanoscale graphitic tubules obtained by MD simulation (Robertson *et al.*[10]) for the elastic shell theory, Yakobson *et al.*[11] proposed the Poisson ratio $v=0.19$, wall thickness $h=0.066$ nm, and Young's modulus $E=5.5$ TPa, respectively. Using shell finite elements with these parameters, Pantano *et al.*[8] reproduced the rippling phenomena observed in previous experiments.[2,3] It should be noted that the equivalent wall thickness $h=0.066$ nm appears to be less than the atomic radius and is much less than the graphite interplanar spacing of 0.34 nm. Actually, it is hard to define the thickness of a single-atom sheet, even more difficult to get the consistent expression for SWNTs and MWNTs.

In this paper, a nonlinear numerical model, membrane-spring model, is proposed based on the physical structure of carbon nanotubes for the simulation of their mechanical response. In this model, CNTs are modeled as a number of membranes joined with rotational springs. The in-plane behavior of the graphite sheet is simulated by the membranes while its bending behavior is modeled by the rotational springs.

II. MODEL OF IN-PLANE BEHAVIOR OF THE GRAPHITE SHEET

We assume that the graphite sheet plane is parallel to the *x-y* plane, and its stress-strain relation[12] is given as follows:

$$\boldsymbol{\sigma} = \boldsymbol{D}\boldsymbol{\varepsilon}, \tag{1}$$

where $\boldsymbol{\sigma}=[\sigma_x\sigma_y\sigma_z\tau_{yz}\tau_{zx}\tau_{xy}]^{\mathrm{T}}$, $\varepsilon=[\varepsilon_x\varepsilon_y\varepsilon_z\gamma_{yz}\gamma_{zx}\gamma_{xy}]^{\mathrm{T}}$, and

$$\boldsymbol{D} = \begin{bmatrix} 1060 & 180 & 15 & 0 & 0 & 0 \\ 180 & 1060 & 15 & 0 & 0 & 0 \\ 15 & 15 & 36.5 & 0 & 0 & 0 \\ 0 & 0 & 0 & 4.5 & 0 & 0 \\ 0 & 0 & 0 & 0 & 4.5 & 0 \\ 0 & 0 & 0 & 0 & 0 & 440 \end{bmatrix} \text{GPa}. \tag{2}$$

It can be concluded from Eqs. (1) and (2) that the graphite sheet has the transverse anisotropic property, so it acts as a membrane rather than a shell.

The in-plane behavior of the graphite sheet can be modeled as

$$\boldsymbol{N}_{\mathrm{m}} = \boldsymbol{D}_{\mathrm{m}}\boldsymbol{\varepsilon}_{\mathrm{m}}, \tag{3}$$

where $\boldsymbol{N}_{\mathrm{m}}=[N_xN_yN_{xy}]^{\mathrm{T}}=[h\sigma_xh\sigma_yh\sigma_{xy}]^{\mathrm{T}}$ is the internal force, $h=0.34$nm is the graphite interplanar spacing. $\boldsymbol{\varepsilon}_{\mathrm{m}}$

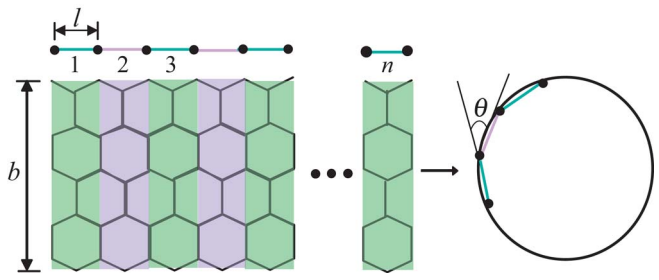

FIG. 1. (Color online) The membrane-spring model of a zigzag tube.

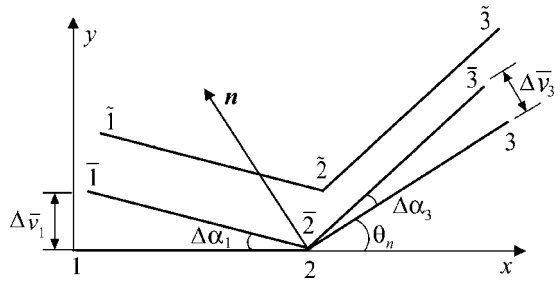

FIG. 2. The 2D model: two bars connected by a spring.

$=[\varepsilon_x \varepsilon_y \varepsilon_{zy}]^{\mathrm{T}}$ is the strain vector, and the in-plane stiffness is

$$\boldsymbol{D}_{\mathrm{m}} = \begin{bmatrix} 360.4 & 61.2 & 0 \\ 61.2 & 360.4 & 0 \\ 0 & 0 & 149.6 \end{bmatrix} \mathrm{N/m}. \tag{4}$$

Note that the elastic matrix of Eq. (2) is the result if the interplanar spacing of graphite is assumed to be $h=0.34$ nm. The in-plane stiffness of Eq. (4) used in our simulation is obtained without any assumption for thickness of the single-atom sheet, namely, the material property for membranes is independent of the representative thickness.

III. MODEL OF BENDING BEHAVIOR OF THE GRAPHITE SHEET

Robertson *et al.*[10] had examined the energetics of all 169 possible graphitic tubules with radius less than 9 Å using both empirical potentials and first-principle total-energy methods. They found that the strain energy per carbon atom relative to an unstrained graphite sheet varies as $1/r^2$ and is insensitive to other aspects of the lattice structure. The strain energy U_c of a tube can be approximated as

$$U_c = \frac{DA_c}{2r^2}, \tag{5}$$

where $D=0.85$ eV$=1.36\times10^{-19}$ J, A_c is the area per carbon atom, and r is the tubule radius.

A. Bar-spring model for 2D problems

A SWNT can be viewed as wrapping one graphite sheet up into a cylinder. Assuming that the axial length is large enough compared to its radius, the deformation in the axial direction can be considered uniform. In addition, it has been reported[10] that the strain energy relative to an unstrained graphite sheet in the wrapping process is insensitive to its chirality. Here, taking a zigzag CNT as an example, the three-dimensional (3D) SWNT of length b can be considered as a 2D ring and modeled as n bars of length l connected by n rotational springs, as shown in Fig. 1. The total strain energy E of the rotational springs is given by

$$E = \tfrac{1}{2}nk\theta^2 = \frac{2\pi^2 k}{n}, \tag{6}$$

where $\theta=2\pi/n$ is the angle of a spring rotated, and k is the spring's stiffness, which is assumed to be independent of the angle's change.

According to Eq. (5), the strain energy per unit area equals $D/2r^2$. Therefore, the total strain energy of the SWNT can be obtained as

$$U = \frac{Dnbl}{2r^2}. \tag{7}$$

As the number of bars increases, the tubule radius r approaches to

$$r = \frac{nl}{2\pi}. \tag{8}$$

The significant deformation from a flat graphite sheet to a CNT is due to the pure bending, thus the deformation of the bars can be ignored comparing to springs. Equating the strain energy E of the springs given in Eq. (6) to the strain energy U of the tubule given in Eq. (7), the equivalent spring stiffness k can be obtained as

$$k = \frac{Db}{l}, \tag{9}$$

which is independent of the tubule radius r. Note that if the length of bars is not uniform, Eq. (9) should be rewritten as

$$k_i = \frac{2Db}{l_i + l_{i+1}}, \tag{10}$$

where l_i and l_{i+1} are the lengths of the adjacent bars attached to the ith spring.

In the 3D shell model, a node has five or six degrees of freedom. In contrast, a node has only three translational degrees of freedom in the 3D membrane-spring model. The rotation of springs can be determined in terms of the displacements of their adjacent membranes. Consequently, the proposed model is not only more similar to the real structure of the CNTs and easier to be coupled with MD simulation, but also more computationally efficient than the shell model.

In order to simulate the nonlinear mechanical behavior of CNTs, an incremental algorithm is used with the updated Lagrangian formulation. Take the 2D model shown in Fig. 2 as an example, bars 12 and 23 are connected by a rotational spring at node 2. Configuration 123 is the one at time step n

(the reference configuration), while $\tilde{1}\tilde{2}\tilde{3}$ is the one at time step $n+1$ (the current configuration). For the sake of convenience in measuring the deformation of the rotational spring at node 2, $\tilde{1}\tilde{2}\tilde{3}$ is translated to the position of $\bar{1}\bar{2}\bar{3}$. $\boldsymbol{n}$ is the normal vector to bar 23. The strain energy of the rotational spring in the current configuration is expressed as

$$V_e = \tfrac{1}{2}k_e\theta_{n+1}^2 = \tfrac{1}{2}k_e(\theta_n + \Delta\alpha_1 + \Delta\alpha_3)^2, \tag{11}$$

where k_e is the elastic stiffness of the rotational spring at node 2, and θ_n is the angle between bar 23 and x axis in the reference configuration, $\Delta\alpha_1$ and $\Delta\alpha_3$ are the incremental angles rotated by bars 12 and 23 during this step, respectively.

Although CNT undergoes large deformation, the incremental displacement in one single time step is generally small. Let $\Delta\boldsymbol{u}=[\Delta u_1 \Delta v_1 \Delta u_2 \Delta v_2 \Delta u_3 \Delta v_3]^{\mathrm{T}}$ denote the incremental displacement vector of nodes 1, 2, and 3 during time step n to $n+1$ in the local reference coordinate system xy. Assuming small displacement, the incremental angles $\Delta\alpha_1$ and $\Delta\alpha_3$ can be approximated as

$$\Delta\alpha_1 \approx \tan\Delta\alpha_1 = \frac{\Delta\bar{v}_1}{l_1}, \tag{12}$$

$$\Delta\alpha_3 \approx \tan\Delta\alpha_3 = \frac{\Delta\bar{v}_3}{l_2}, \tag{13}$$

where $\Delta\bar{v}_1=\Delta v_1-\Delta v_2$,

$$\Delta\bar{v}_3 = [n_x\ n_y]\begin{Bmatrix}\Delta u_3 - \Delta u_2\\ \Delta v_3 - \Delta v_2\end{Bmatrix},$$

$n_x=-\sin(\theta_n)$, and $n_y=\cos(\theta_n)$ are the direction cosine of the normal vector $\boldsymbol{n}$. l_1 and l_2 are the length of bars 12 and 23 in the reference configuration, respectively.

Substituting Eqs. (12) and (13) into Eq. (11), the strain energy of the spring can be rewritten as

$$V_e = \tfrac{1}{2}k_e\left[\theta_n + \frac{1}{l_1}\Delta v_1 + \frac{\sin\theta_n}{l_2}\Delta u_2 - \left(\frac{1}{l_1}+\frac{\cos\theta_n}{l_2}\right)\Delta v_2 - \frac{\sin\theta_n}{l_2}\Delta u_3 + \frac{\cos\theta_n}{l_2}\Delta v_3\right]^2 = \tfrac{1}{2}k_e[\theta_n + \boldsymbol{B}\Delta\boldsymbol{u}]^2, \tag{14}$$

where

$$\boldsymbol{B} = \left[0\ \frac{1}{l_1}\ \frac{\sin\theta_n}{l_2}\ -\left(\frac{1}{l_1}+\frac{\cos\theta_n}{l_2}\right)\ -\frac{\sin\theta_n}{l_2}\ \frac{\cos\theta_n}{l_2}\right].$$

Applying the Castigliano's theorem to Eq. (14) leads to

$$\frac{\partial V_e}{\partial\Delta\boldsymbol{u}} = \boldsymbol{K}_e\Delta\boldsymbol{u} + \boldsymbol{F}_e, \tag{15}$$

where

$$\boldsymbol{K}_e = k_e\boldsymbol{B}^{\mathrm{T}}\boldsymbol{B}, \tag{16}$$

$$\boldsymbol{F}_e = k_e\theta_n\boldsymbol{B}^{\mathrm{T}}. \tag{17}$$

In Eqs. (16) and (17), $\boldsymbol{K}_e$ and $\boldsymbol{F}_e$ are the stiffness matrix and the initial internal stress vector at time step n, respectively.

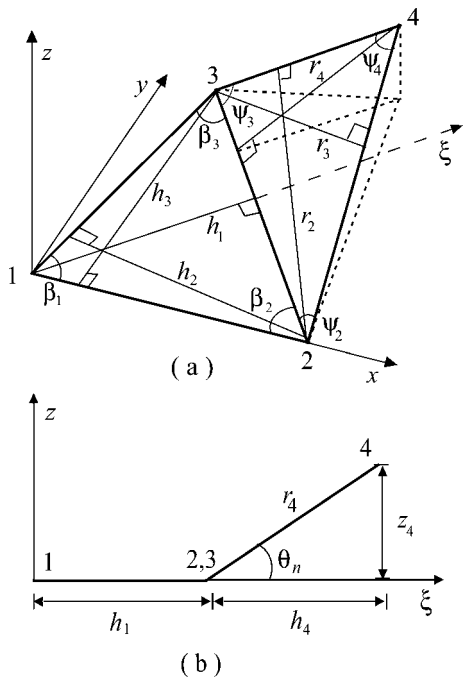

FIG. 3. (a) Two membranes connected by a spring, and their geometric parameter, (b) the configuration in the plane normal to spring 23.

B. Membrane-spring model for 3D problems

Consider Fig. 3(a), where two adjacent membranes 123 and 432 are connected by a rotational spring along side 23. In the ξ-z plane normal to spring 23, as shown in Fig. 3(b), the rotation angle of spring 23 in the reference configuration can be expressed in term of the position of nodes 1–4 as

$$\theta_n = \cos^{-1}\left(\frac{h_4}{r_4}\right), \tag{18}$$

where r_4 is the altitude from node 4 to side 23 and h_4 is the projection of r_4 in the x-y plane.

Because the rotation angle of the spring is independent of the translation of its adjacent membranes, the translation of the membranes can be ignored in the following analysis. To measure the rotation angle of facets 123 and 234 along side 23, a translation of the facet brings node $\bar{2}$ to 2, and then a rotation of segment $\bar{2}\bar{3}$ around the fixed node 2 in vertical plane makes line $\bar{2}\bar{3}$ match together with 23. At this time, nodes 3 and 4 are also moved, but the angle of facets 123 and 234 would not be changed. Figure 4 shows the current (at time $t=t_{n+1}$) and the reference (at time $t=t_n$) configurations in the ξ-z plane. Assuming $\{\Delta u_i, \Delta v_i, \Delta w_i\}$ are the incremental displacements of node i in the local reference coordinate system xyz. Thus the incremental angles $\Delta\alpha_1$ and $\Delta\alpha_4$ can be calculated by

$$\Delta\alpha_1 \approx \frac{\Delta\bar{w}_1}{h_1} = \left[\frac{1}{h_1}\ -\frac{\cos\beta_3}{h_2}\ -\frac{\cos\beta_2}{h_3}\right]\begin{Bmatrix}\Delta w_1\\ \Delta w_2\\ \Delta w_3\end{Bmatrix}, \tag{19}$$

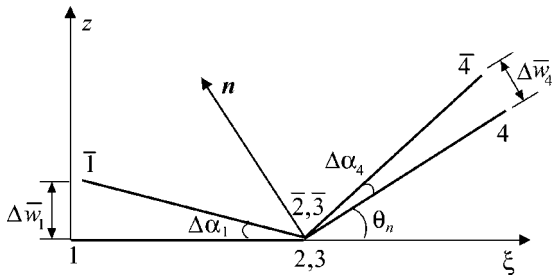

FIG. 4. Current and reference configurations in the ξ-z plane.

$$\Delta\alpha_4 \approx \frac{\Delta\bar{w}_4}{r_4} = \left[-\frac{\cos\psi_3}{r_2} \quad -\frac{\cos\psi_2}{r_3} \quad \frac{1}{r_4} \right] \begin{Bmatrix} \Delta w_2' \\ \Delta w_3' \\ \Delta w_4' \end{Bmatrix}, \quad (20)$$

where

$$\Delta w_2' = \Delta \boldsymbol{u}_2 \cdot \boldsymbol{n} = \Delta u_2 n_x + \Delta v_2 n_y + \Delta w_2 n_z,$$

$$\Delta w_3' = \Delta \boldsymbol{u}_3 \cdot \boldsymbol{n} = \Delta u_3 n_x + \Delta v_3 n_y + \Delta w_3 n_z,$$

$$\Delta w_4' = \Delta \boldsymbol{u}_4 \cdot \boldsymbol{n} = \Delta u_4 n_x + \Delta v_4 n_y + \Delta w_4 n_z, \quad (21)$$

and $\boldsymbol{n}=[n_x n_y n_z]^{\mathrm{T}}$ is the normal vector to the facet 234 in the local coordinate system xyz. Other parameters are defined in the Figs. 3(a) and 4. The derivation of $\Delta\alpha_1$ and $\Delta\alpha_4$ are given in detail in Ref. 13 to establish a new DKT element.

Thus the energy of the rotational spring alone side 23 can be expressed as

$$\begin{aligned} V_e &= \tfrac{1}{2}k_e(\theta_n + \Delta\alpha_1 + \Delta\alpha_4)^2 \\ &= \tfrac{1}{2}k_e\Bigg[\theta_n + \frac{1}{h_1}\Delta w_1 - \frac{\cos\psi_3 n_x}{r_2}\Delta u_2 - \frac{\cos\psi_3 n_y}{r_2}\Delta v_2 \\ &\quad - \left(\frac{\cos\beta_3}{h_2} + \frac{\cos\psi_3 n_z}{r_2}\right)\Delta w_2 - \frac{\cos\psi_2 n_x}{r_3}\Delta u_3 \\ &\quad - \frac{\cos\psi_2 n_y}{r_3}\Delta v_3 - \left(\frac{\cos\beta_2}{h_3} + \frac{\cos\psi_2 n_z}{r_3}\right)\Delta w_3 \\ &\quad + \frac{n_x}{r_4}\Delta u_4 + \frac{n_y}{r_4}\Delta v_4 + \frac{n_z}{r_4}\Delta w_4 \Bigg]^2 \\ &= \tfrac{1}{2}k_e[\theta_n + \boldsymbol{B}\Delta\boldsymbol{u}]^2, \end{aligned} \quad (22)$$

where $\boldsymbol{B}$ is defined by

$$\boldsymbol{B} = [\boldsymbol{B}_1 \quad \boldsymbol{B}_2 \quad \boldsymbol{B}_3 \quad \boldsymbol{B}_4], \quad (23)$$

$$\boldsymbol{B}_1 = \left[0 \quad 0 \quad \frac{1}{h_1} \right],$$

$$\boldsymbol{B}_2 = \left[-\frac{\cos\psi_3 n_x}{r_2} \quad -\frac{\cos\psi_3 n_y}{r_2} \quad -\left(\frac{\cos\beta_3}{h_2} + \frac{\cos\psi_3 n_z}{r_2}\right) \right],$$

$$\boldsymbol{B}_3 = \left[-\frac{\cos\psi_2 n_x}{r_3} \quad -\frac{\cos\psi_2 n_y}{r_3} \quad -\left(\frac{\cos\beta_2}{h_3} + \frac{\cos\psi_2 n_z}{r_3}\right) \right],$$

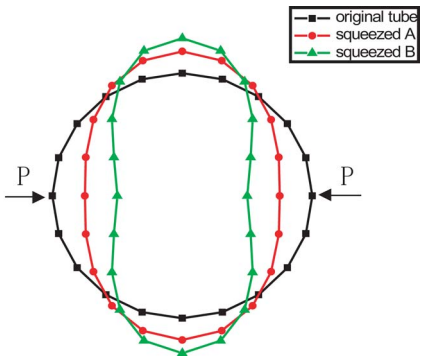

FIG. 5. (Color online) Original and squeezed configurations obtained with the membrane-spring model.

$$\boldsymbol{B}_4 = \left[\frac{n_x}{r_4} \quad \frac{n_y}{r_4} \quad \frac{n_z}{r_4} \right].$$

Applying the Castigliano's theorem to Eq. (22) results in a similar equation to Eq. (15).

The equilibrium configuration can be obtained by minimizing the total energy of the membranes and springs. Pantano *et al.*[8] used an interaction element to simulate the van der Waals forces, which is necessary when simulating MWNT deformations, and tube-tube or tube-substrate interactions. It can be included in our model. Thus, both the small and large deformation mechanical responds of carbon nanotubes can be analyzed using the membrane-spring model.

IV. NUMERICAL EXAMPLES

Finite element analysis program (FEAP) (Ref. 14) is a general purposed finite element analysis code, which is designed for research and educational use. To implement the membrane-spring model, user subroutines are added in FEAP. To validate the proposed membrane-spring model, several examples are analyzed and the numerical results are compared with those obtained using other methods.

A. Radial compression

A (32,0) zigzag nanotube with a 2.54 nm diameter[15] is considered. This system consists of 384 atoms. In our 2D simulation only 20 nodes with 40 degrees of freedom are used, which is substantially less than that of the atomic system. The structure is fully relaxed at first. Its equilibrium configuration is obtained by minimizing the total energy, including springs and bars. The structure is then subjected to the following two load cases, respectively. (1) Squeezed A: The tube is squeezed to $\frac{3}{4}$ of its original size along one diameter; (2) Squeezed B: The tube is squeezed to $\frac{1}{2}$ of its original size along one diameter.

Figure 5 shows the original configuration and the final ones of different load cases. To compare with the results of molecular mechanics (MM),[15] the equilibrium configuration with 64-node in the squeezed B case is shown in Fig. 6. The numerical result agrees well with that obtained by MM.

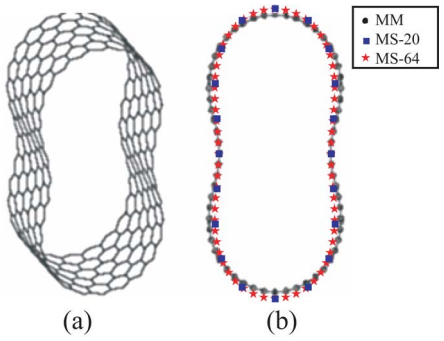

FIG. 6. (Color online) (a) Actual molecular model (Ref. 15), (b) the final configuration obtained by MM (black circle) (Ref. 15), and the results of the proposed model with 20 nodes (square) and 64 nodes (star).

B. Wrapping process

The wrapping process of CNT is reproduced in this example to further validate the proposed model. Assuming that the deformation is uniform in the axial direction, the 2D model including 20 bars joined by springs is used to model the tube in the wrapping process. Figure 7 shows the sequences of the process in different time steps, which is consistent with the 2–8 configurations of Fig. 8 in the reference article[16] before considering the van der Waals force.

C. Axially compressed buckling

The buckling analysis under axial compression is one focus of the CNTs' mechanical behaviors. Using MD simulation, Yakobson *et al.*[11] found four shape changes with the increase of axial strain, Fig. 9 displayed the configurations of buckling. Liu *et al.*,[17] using the atomic-scale finite element method, also obtained the bifurcation pattern similar to Fig. 9(c) and the corresponding strain is 0.07. In addition, Liew *et al.*[18] examined the effects of the number of layers on the MWNT and found the optimum diameter for SWNT through studying the buckling behavior of SWNTs and MWNTs under axial compression. In another work,[19] the buckling behavior of carbon nanotube bundles was carried out using MD simulation.

A (7,7) armchair CNT under compression is investigated using the membrane-spring model of 656 nodes. In order to compare with the result of Yakobson *et al.*,[11] the CNT in this simulation has the same geometry properties of length L =6 nm and diameter d=1 nm. The material parameters of the model are determined according to Eqs. (4) and (10). Using the nonlinear static analysis, the first two bulking configurations are obtained, as shown in Fig. 10, which are in good agreement with the previous results of MD simulation. With the increase of axial compression, the stiffness matrix becomes singularity. Therefore, it is almost impossible to obtain the next converged buckling configuration.

To overcome the difficulties associated with the singularity of the stiffness matrix in the static analysis, a nonlinear dynamic analysis is performed, whose Newmark-β formulation[14] is given by

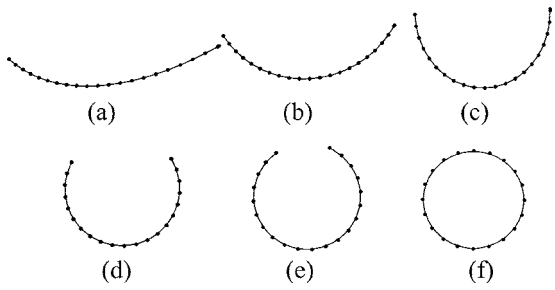

FIG. 7. Selected frames of a video recording of wrapping process.

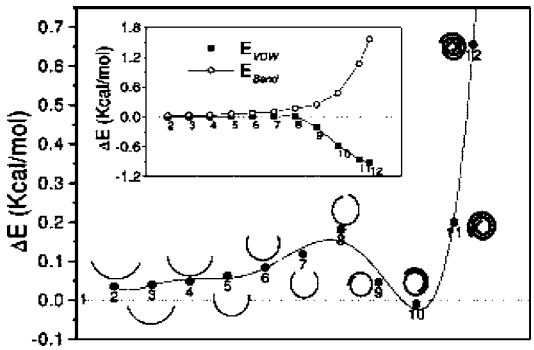

FIG. 8. Change in energy and the according configurations during a single graphite sheet to make a CNS (carbon nanoscroll) (Ref. 16).

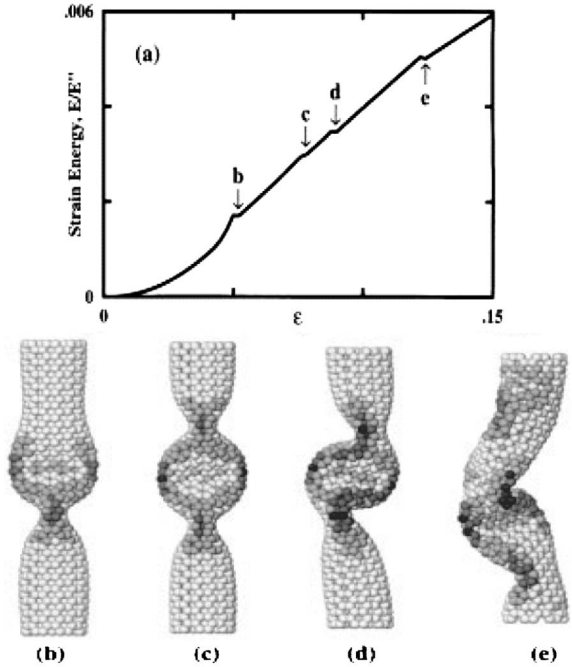

FIG. 9. (a) The change of strain energy corresponding to the different axial strain, (b)–(d) display the four buckling configurations at the stages indicated in (a) with the strain of 0.05, 0.076, 0.09, 0.13 respectively (Ref. 11).

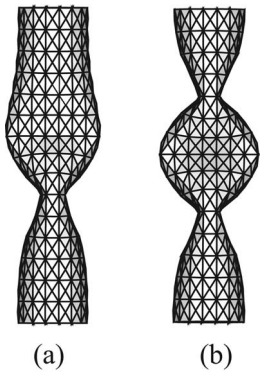

FIG. 10. The buckling configurations obtained by the nonlinear static analysis (a) $\varepsilon=0.05$, (b) $\varepsilon=0.086$.

$$\left(\boldsymbol{K}+\frac{1}{\alpha\Delta t^2}\boldsymbol{M}+\frac{\delta}{\alpha\Delta t^2}\boldsymbol{C}\right)\Delta\boldsymbol{u}_{t+\Delta t}=\boldsymbol{Q}_{t+\Delta t}. \tag{24}$$

where $\boldsymbol{K}$, $\boldsymbol{M}$, $\boldsymbol{C}$ are the stiffness, mass, and damping matrix, respectively. $\boldsymbol{Q}_{t+\Delta t}$ is the efficient load at time $t+\Delta t$. α, δ are the specific parameters used in Newmark-β method. It can be seen from Eq. (24) that the singularity of stiffness matrix can be eliminated by considering the effect of inertia and damping. The simulation is divided into two phases. In the first run, large load steps are carried out to obtain the possible critical points through the change of strain and kinetic energy with the axial strain. In the second run, smaller load steps are applied near before the critical point and a stage of time holding the load is needed after the formation of buckling configuration to decrease the kinetic energy. On the other hand, the rate of convergence supplies the additional information to obtain the buckling and post-buckling configurations. Figure 11 shows the obtained buckling configurations, where the first two configurations are nearly the same as those obtained by the static analysis. The asymmetric configuration is obtained at the axial strain of 0.11. The tube collapses at the axial strain of 0.12. It should be noted that the van der Waals forces are not included in the present simulation. Therefore, the tube wall is almost in self contact in Fig. 11(e), which greatly decrease the stiffness of CNTs.

V. CONCLUSIONS

An efficient model is proposed based on its physical microstructure for the numerical simulation of carbon nanotube. CNTs are modeled as membranes connected by rotational springs, eliminating the requirement to define the equivalent wall thickness of CNTs. In this model, every node has three translational degrees of freedom in three-dimension space, which substantially decreases the computation cost compared to the shell model. In addition, the model is easily coupled with MD simulation to develop a multiscale model. The numerical results obtained by the proposed model are in good agreement with those of MD simulation.

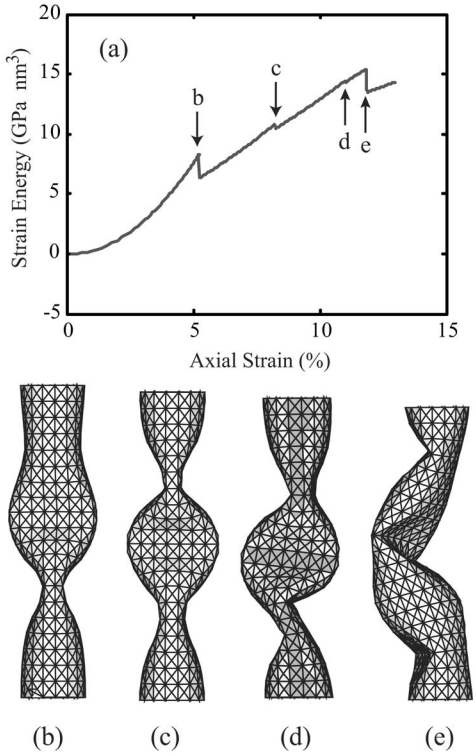

FIG. 11. (a) Variation of strain energy with the axial strain, (b)–(e) display the four buckling configurations obtained by the dynamic analysis, whose corresponding strain $\varepsilon=0.0525$, 0.083, 0.11, 0.12 respectively.

ACKNOWLEDGMENT

The authors acknowledge the financial support for this work from the National Basic Research Program of China through Grant No. 2004CB619304.

*Electronic address: xzhang@tsinghua.edu.cn

[1] M. M. J. Treacy, T. W. Ebbesen, and J. M. Gibson, Nature (London) **381**, 678 (1996).
[2] E. W. Wong, P. E. Sheehan, and C. M. Lieber, Science **277**, 1971 (1997).
[3] P. Poncharal, Z. L. Wang, D. Ugarte, and W. de Heer, Science **283**, 1513 (1999).
[4] J. P. Salvetat, G. A. Briggs, J. M. Bonard, R. R. Bacsa, A. J. Kulik, T. Stockli, N. A. Burnham, and L. Forro, Phys. Rev. Lett. **82**, 944 (1999).
[5] M. F. Yu, O. Lourie, M. J. Dyer, K. Moloni, T. F. Kelly, and R. S. Ruoff, Science **287**, 637 (2000).
[6] K. M. Liew, X. Q. He, and C. H. Wong, Acta Mater. **52**, 2521 (2004).
[7] K. M. Liew, C. H. Wong, X. Q. He, and M. J. Tan, Phys. Rev. B **71**, 075424 (2005).
[8] A. Pantano, M. C. Boyce, and D. M. Parks, Phys. Rev. Lett. **91**, 145504 (2003).

[9] M. Arroyo and T. Belytschko, Phys. Rev. Lett. **91**, 215505 (2003).
[10] D. H. Robertson, D. W. Brenner, and J. W. Mintmire, Phys. Rev. B **45**, 12592 (1992).
[11] B. I. Yakobson, C. J. Brabec, and J. Bernholc, Phys. Rev. Lett. **76**, 2511 (1996).
[12] B. T. Kelly, *Physics of Graphite* (Applied Science, London, 1981).
[13] Y. Q. Guo, W. Gati, H. Naceur, and J. L. Batoz, Comput. Struct. **80**, 2299 (2002).
[14] O. C. Zienkiewicz and R. L. Taylor, *The Finite Element Method*, 5th ed. (Butterworth-Heinemann, Oxford, 2000), Vol. 1-3.
[15] M. Arroyo and T. Belytschko, Mech. Mater. **35**, 193 (2003).
[16] S. F. Braga, V. R. Coluci, S. B. Legoas, R. Giro, D. S. Galcao, and R. H. Baughman, Nano Lett. **4**, 881 (2004).
[17] B. Liu, Y. Huang, H. Jiang, S. Qu, and K. C. Hwang, Comput. Methods Appl. Mech. Eng. **193**, 1849 (2004).
[18] K. M. Liew, C. H. Wong, X. Q. He, M. J. Tan, and S. A. Meguid, Phys. Rev. B **69**, 115429 (2004).
[19] K. M. Liew, C. H. Wong, and M. J. Tan, Appl. Phys. Lett. **87**, 041901 (2005).